Journal of
Renewable Energy Research and Applications (RERA)

Vol 2. No 1, 2021, 1-8 *DOI: 10.22044/RERA.2020.9778.1037*

Design of Solar-powered Endurance Glider with Vortex Generators

Sh. Sham Dol*, S. Shahid Pervaiz, M. Uzair, Sharaez Khalid Bashir and M. Mustafa Elzughb

Department of Mechanical Engineering, Abu Dhabi University, Abu Dhabi, United Arab Emirates.

Received Date 29 June 2020; Revised Data 23 July 2020; Accepted Date 26 October 2020
**Corresponding author: sharulshambin.dol@adu.ac.ae*

Abstract
This research work aims at designing a solar endurance glider for an increased flight time. The constraints for the design include reduction in weight compared to a typical glider, and improving its aerodynamic performance by application of the vortex generators on its wingspan. The design of each component is performed through various stages of similitude cases; furthermore, the components such as the solar panels and vortex generators are selected based on a decision matrix design process. This research work utilizes the ANSYS 18.1 K-Omega SST turbulence simulation techniques in order to successfully simulate the glider at different speeds along with various angles of attack for the aerodynamics optimization. The results obtained show an improvement in the lift force from 160 N to 192 N once the vortex generators are installed. 16 solar cells are installed on the glider's wings, providing 57.6 Watts of power. This work faces a limitation on the physical testing using a wind tunnel for validation; therefore, the team relies on the CFD simulation verification from the published data. This report details the concepts of boundary layer, design process, and glider simulation as well as the glider configurations such as the wingspan and total length. The glider should be able to maintain a flight time of at least 6 hours with vortex generators and solar panels.

Keywords: *Vortex Generators, Solar Panels, Glider, Coefficient of Lift, Coefficient of Drag, Boundary Layer.*

1. Introduction

Unmanned aerial vehicles (UAVs) have been the center of research works for several decades; now the emphasis has been shown on providing a medium for communication and surveillance through the use of high-altitude long endurance (HALE) UAVs. There are numerous aircrafts today that can uphold prolonged periods of flight time; however, an extensive and sustainable flight time is always something to pursue. In the recent years, a lot of research works have been centered on the solar power and its potential as an alternative power source.

Depending on the application, the glider should be capable of a consistent uninterrupted flight. Saif Eldin and Dol [1] have highlighted some applications of the aerial vehicles such as a UAV, which is able to deliver a floatation device for drowning offshore workers under a variety of weather conditions. Similarly, Hassanalian and Abdelkefi in [2] have mentioned the military surveillance and planetary exploration as the potential applications of UAVs. However, this can be quite impractical when considering the conventional air propulsion systems, and thus focusing on more sustainable forms of energy generation such as solar power becomes more imperative. Taking into account a proper design and varying climate and thermal conditions, a solar powered aircraft could potentially fly for an excessive amounts of time [3]. Figure 1 illustrates the Solong glider, which has an efficiency of 21.5% and is able to fly for 48 hours without landing [4].

Figure 1. A Solong Glider [4].

A major constraint to the work around when designing an airborne vehicle is flow separation,

which induces high energy losses and is excessively detrimental to a system that does not have the luxury to expend more power than necessary. Boundary layer separation, in the elementary terms, occurs when a high-speed flow separates due to an adverse pressure gradient when the flow is expanded due to a trailing edged surface, in this case, an airfoil [5].

In an attempt to minimize the energy losses, the concept of Vortex Generators (VGs) has been employed. VGs are protrusions, indentations, contraptions or added alterations on a surface that as the name implies induce vortices. These vortices work to energize the freestream flow, encouraging the mixing of higher freestream velocity and lower air velocity within the boundary layer, leading to the "re-attaching" of separated flow or, ideally, the prevention of flow separation all together [6]. The purpose of all of these works is to augment the lift performance [7]. This project attempts to manufacture a "perpetual flight" by implementing vortex generators across the wingspan of a solar powered endurance glider; these are hypothesized to enhance the aerodynamic performance of the glider, ultimately increasing the flight time by lowering drag on the glider surface. The simulation is conducted using a finite element analysis through ANSYS Fluent, K-Omega SST turbulence CFD model.

2. Design

The lift and drag are the main forcers governing the behavior of an aircraft. When considering an airfoil, there are two points of focus on: the stagnation point or leading edge and the trailing edge, as shown in figure 2 [8,9].

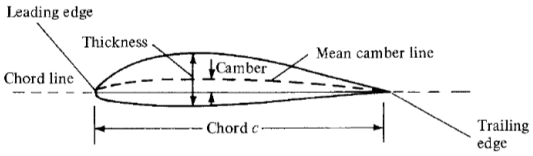

Figure 2. Airfoil Nomenclature [9].

The leading edge divides the freestream flow between the upper and lower surfaces, and the divided flow is rejoined at the trailing edge. Consider two particles from the freestream, split at the leading edge and reunited at the trailing edge. The average velocity of the particle on the upper surface tends to be higher than that of the one on the lower surface. In reference to Bernoulli's Equation (1), this would imply that there is a pressure difference, and this difference in pressure between the upper and lower surfaces is the direct cause of the lift force [10];

$$P_1 + \frac{1}{2}\rho {V_1}^2 + \rho g z_1 = P_2 + \frac{1}{2}\rho {V_2}^2 + \rho g z_2 \quad (1)$$

Drag is basically the resistance to motion due to an object's shape, material, and speed. The lift-to-drag ratio is an important parameter, as it is used to determine the airfoil efficiency [11-13]. The followings are the equations for the lift and drag forces:

$$L = \frac{1}{2} C_L V^2 \rho S \quad (2)$$

$$D = \frac{1}{2} C_D V^2 \rho S \quad (3)$$

$$\frac{L}{D} = \frac{C_L}{C_D} \quad (4)$$

The design was conducted using a function decomposition method, and each sub-component of the design was thoroughly assessed using a decision matrix in order to determine the optimal structure for this research work. The decision matrix using the info from [14] for selecting the wing shape is shown in table 1.

Table 1. Decision matrix for wing shape.

0 = Poor | 1 = Satisfactory | 2 = Reasonable | 3 = Very Good | 4 = Excellent

	Wing Shape			
Criteria	**Elliptical wing**	**Rectangular wing**	**Tapered wing**	**Swept wing**
Lift coefficient	2	3	4	2
Drag reduction	4	1	3	0
Ease of manufacturing	0	4	2	2
Cost	1	3	2	2
Strength	3	2	3	2
Stall resistance	2	1	2	3
Total	12	14	16	11

2.1. Solar Panel

There are a variety of solar panels available in the market, and choosing the most efficient one is essential for the research project. The decision matrix shown in table 2 summarizes the final solar panel selected for the project:

Table 2. Decision matrix for solar panels.

0 = Poor | 1 = Satisfactory | 2 = Reasonable | 3 = Very Good | 4 = Excellent

	Solar panels			
Criteria	**KK-moon solar panel**	**Jiang Flexible solar cell**	**Sunpower maxeon solar cells**	**Monocrystalline solar cells**
Efficiency	2	1	3	1
Weight	1	3	3	2
Cost	0	2	2	3
Flexibility	0	3	3	0
Ease of use	0	3	2	1
Total	3	12	13	7

The sun power Maxeon solar cells (figure 3) are monocrystalline cells with a high efficiency and performance. They are of the N type, which are doped with phosphorous to make the cell negatively charged. The benefit of the N type is that it is resistant to the boron-oxygen defects that can reduce the efficiency, and it is not affected by light induced degradation [15].

The corners of the solar panels are rounded since the panels are cut from a cylindrical silicon crystal. Because this manufacturing produces less amount of weight, the cost of the solar panels is also reduced due to this. The calculation below basically looks into how many solar panels can be placed on the wingspan of the glider:

$$L_t = 998.83 \cdot 2 = 1997.66 \text{ mm} \quad (5)$$

$$L_s = 125 \text{ mm} \quad (6)$$

$$N_s = \frac{L_t}{L_s} = \frac{1997.66}{125} = 15.9 \text{ cells} \quad (7)$$

$$\text{Number of Solar Cells} \approx 16 \text{ cells}$$

where:

L_t is the total wingspan
L_s is the length per solar cells
N_s is the number of solar cells per wingspan

In order to distribute the weight of the cells equally, 16 cells are placed in series with 8 per wing. The power rating of each cell is given as 3.6 Watts so the total power coming from the cells will be:

$$\dot{W}_t = 16 \times 3.6 = 57.6 \text{ W} \quad (8)$$

$$V_t = 16 \times 0.55 = 8.8 \text{ V} \quad (9)$$

More solar cells can be attached to the wingspan in order to provide a higher voltage that technically depends upon the battery that is being used for the glider. Figure 3 shows the chosen sun power Maxeon solar cells.

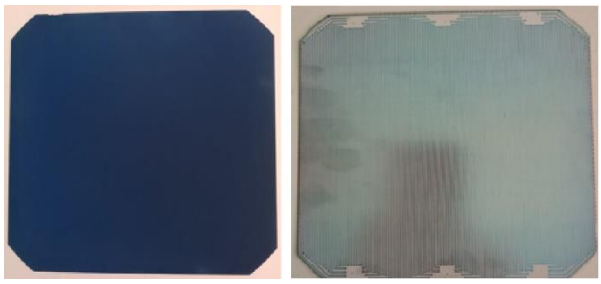

Figure 3. Sun power Maxeon solar cells.

The battery selected is a 2200mAh, 2s (2 cell) Li-Po one with a weight of 135 g. 2s batteries have a total voltage of 7.4, which is lower than the output voltage from the solar cells. With the aid of the MPPT solar charge controller, the glider should be able to maintain a flight time of at least 6 hours as the power drawn by the motor to maintain flight is not more than 2 Amps. The lift generated from thermals (pockets of hot air rising from the ground) also adds the lift force to the glider, allowing for little to no power usage from the propeller giving the Li-po battery more time to charge.

2.2. Vortex Generator

Vortex Generators come in all shapes and sizes, which implies for a decision matrix in order to select the perfect one for the glider. Table 3 breaks down the criteria selected for the specific glider as well as the score on which the criteria are based upon. Each VG has been rated according to various literatures and recorded experimentation on wind turbine blades.

Table 3. Decision matrix for vortex generator.

0 = Poor | 1 = Satisfactory | 2 = Reasonable | 3 = Very Good | 4 = Excellent

	Vortex generator			
Criteria	**Rectangular VG**	**Gothic VG**	**Triangular VG**	**Paraboloic VG**
Pressure and friction drag	1	2	3	2
Lift force	3	2	2	1
Ease of manufacturing	3	0	3	1
Total	7	4	8	4

The decision matrix shown in table 3 proceeded to lead the triangular vortex generator as the best one out of them all with a total of 8 points followed by the rectangular VG with 7 points. The dimensions for the triangular VG have been similitude from [2] through the use of equations. Figure 4 shows the modelled Triangular VG in ANSYS Spaceclaim.

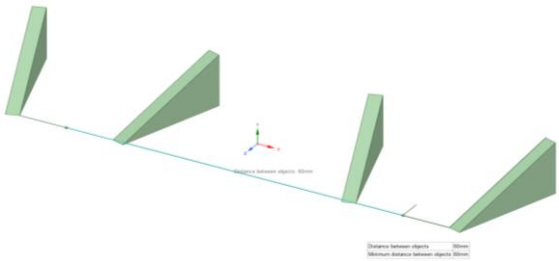

Figure 4. Final design of the vortex generator.

3. Final Design

Weight is the most important variable in a design of an aircraft; therefore; table 4 breaks down the weight distribution of the glider per component. The weight for the entire glider was assumed to be 1160 g as the design matched the Volantex

Phoenix 2400 mm glider and so must the weight. Adding the weight of the other components rounded the total weight to 1587 g that satisfied the weight limit of 4000 g.

Table 4. Components along with their respective weight.

Item	Total weight (g)
Volantex Phoenix 2400mm glider	1160
Lixada 30A MPPT solar charge controller	159
1S 3.7V 500mAh Li-Po battery	13.6
2S 7.4V 2200 mAh Li-Po battery	135
Quantum FPVMe HD Mini Camera	7.4
SunPower c60 solar cells (16 cells)	112
Total flying weight	**1587**

The glider has a wingspan of 2.4 m with a length of 1.2 m. The S1223 selected airfoil provides a higher lift and a less drag compared to the other airfoils. The motor is a brushless 35 Amp motor with a rating of 1050 kV (rpm/volt). The selected propeller is of model 1060 with a diameter of 10 inches and pitch of 6 inches. Technically, a higher pitch provides a higher speed but at the expense of efficiency at lower speeds [16].

The wings are manufactured with EPO foam, while the fuselage is built of the ABS plastic. The ABS plastic can be easily machined, sanded, and glued, which makes it a perfect material for prototyping. The EPO foam is a lightweight durable material with a better surface finish for reduction in skin friction drag.

Figure 5 shows the final glider model modelled in ANSYS Spaceclaim derived from the detailed design above, whilst figure 6 shows the corresponding glider prototype with 16 SunPower Maxeon solar cells. It has the ability to fly up to 6 hours with a weight limit of 4 kg including the payload.

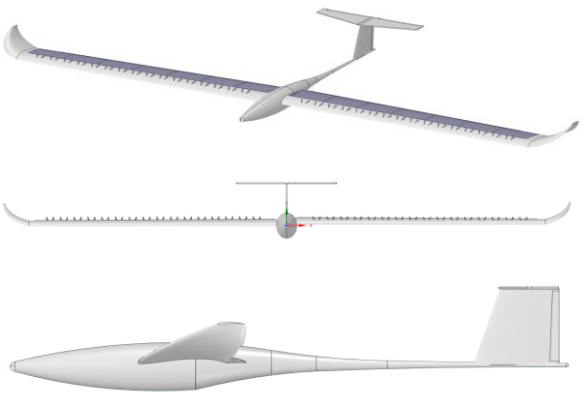

Figure 5. Final design of the glider.

Figure 6. Complete glider prototype.

4. Simulation

The computational analysis was performed on ANSYS Fluent that utilized the SST (Shear Stress Transformation) K-omega turbulence model in order to ensure an accurate representation of flow separation and vortices. SST k-omega is a hybrid model that combines the Wilcox k-omega and the k-epsilon model together. The Wilcox k-omega model governs the flow near the wall, while k-epsilon manages the free stream flow. SST of the turbulence kinetic energy equation in the turbulence model is represented as [17]:

$$\frac{\partial k}{\partial t} + U_j \frac{\partial k}{\partial x_j} = P_k - \beta * k\omega + \frac{\partial}{\partial x_j}[(v + \sigma_k v_T)\frac{\partial k}{\partial x_j}] \quad (10)$$

4.1 Model verification

A simple verification “experiment” was carried out in order to ascertain the validity of the yielded results. With the same model used for the glider, a simple sphere was exposed to air at a certain freestream velocity to verify if the model generated the same coefficient of drag as an already verified graph of graph of drag and Reynolds number yielded, as shown in figure 7 and table 5 [18]. As illustrated in table 5, the coefficient of drag yielded is very close to the verified value, and thus the model can be verified.

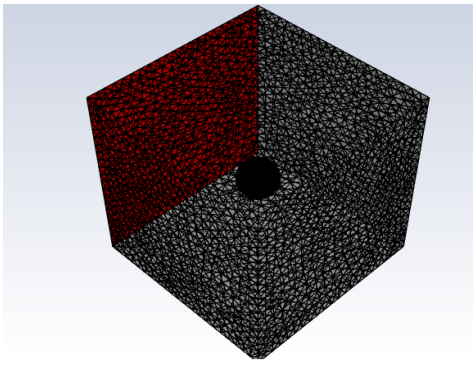

Figure 7. Sphere in mesh enclosure.

Table 5. Results of model verification.

	Re	C_D
Verified	10^5	0.6
Experimental	10^5	0.645

4.2 Glider simulation

In order to gain a more accurate frame for comparison, the simulation was done with just the wing, the wing with winglet, the wing with winglet and VG, and the glider with winglet and VG. The glider was simulated for half the side as it was a symmetrical glider.

Figure 8 shows the mesh of the cross-section of the glider that has 1270353 elements, which comparatively lies on the lower end of the mesh independency. The discretization of the model started off with an unstructured mesh after which it was refined manually. The refining of the mesh was carried out in areas where the mesh density would have had a significant impact on the accuracy of results and it must be able to cover the glider's main features such as the wings, VGs, fuselage, and wake regions.

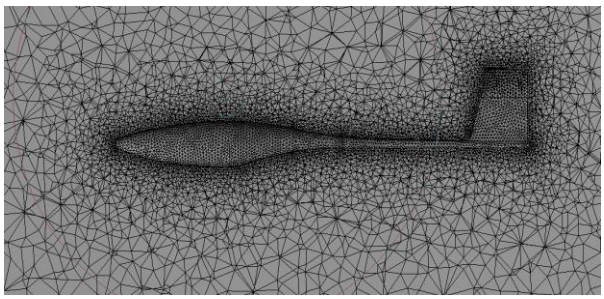

Figure 8. Glider cross-section mesh.

Figure 9 illustrates the pressure distribution on the glider surface at a 0° angle of attack. Freestream air comes into contact with the glider, which is assumed to be fixed in air but it is equivalent to the glider moving in space [19]. The figure shows the more positive pressure regions rather than the negative pressure regions.

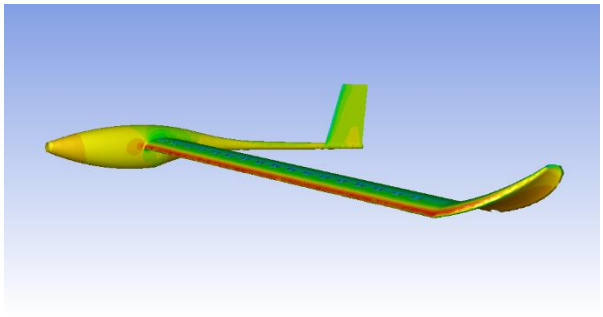

Figure 9. Pressure contour of aircraft at a 0° angle of attack.

The pressure is extreme at the leading edge as the free stream velocity comes into contact at a full force; however, the lower surface generally carries the positive pressure, and the design factors such as the weight tend to drag the wing downwards [19]. For each change in the angle of attack, the pressure distribution varies on the aircraft; therefore, the relative pressure difference results in a lifting force. The center of pressure distribution shifts location once the angle of attack changes.

Figure 10 illustrates the velocity distribution on the glider surface. The velocity downstream decreases gradually and then moves on to the trailing edge where it loses potential. The velocity at the lower surface is similar but has a lower quality compared to the velocity at the top surface. According to the Bernoulli's equation, an increase in velocity is a decrease in pressure [19]. The velocity at the top surface is higher at a price of lower pressure, while the pressure on the bottom side is higher with a lower velocity. As the angle of attack shifts, the velocity on the upper surface increases, while on the bottom surface decreases causing an increase in the pressure distribution and thus creating lift.

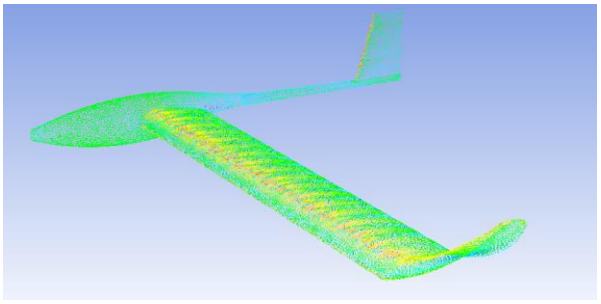

Figure 10. Velocity contour of aircraft at a 0° angle of attack.

The most important aspect of designing a glider is to control the flow separation with respect to the drag reduction. Generally, the flow separation begins to occur at a small angle of attacks, while the flow that is attached to the surface is still dominant. Separation of the boundary layer causes large energy losses that has an adverse effect on the aerodynamic load by reducing the lift and increasing the drag. Figure 9 shows the pressure distribution on VGs that assist the boundary layer to stay attached little longer.

5. Results

The results were taken for the angles of attack (AOA) of 0°, 2°, and 4°. As shown in figure 11, the glider has increased the lift performance due to the added winglet and vortex generators.

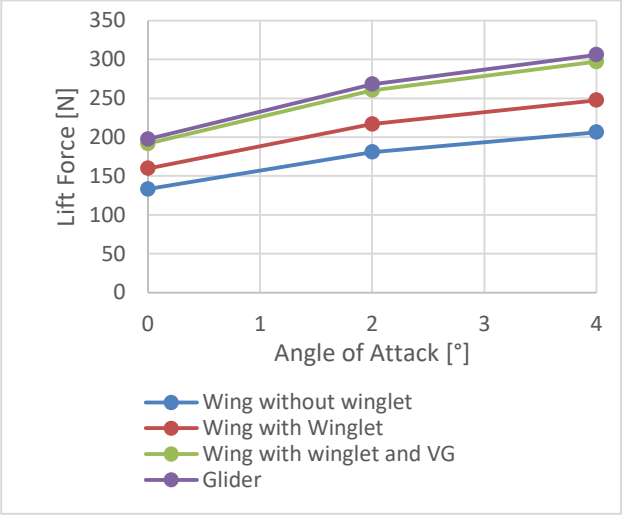

Figure 11. Lift force *vs.* AOA.

Following the above figure, it can be observed that as the angle of attack increases, the lift force increases substantially from 0° to 2° but this increment in the lift force does not continue for long, and eventually comes to a slope with a decrease in lift once the critical angle of attack is reached. Figure 11 illustrates the increase in the lift force as each component is added to the glider such as the winglet and vortex generators. The lift force increased from 216.82 N to about 267.997 N once VGs were implemented on the winglet surface of the glider. The entire glider showed an improvement in the lift force from 267.99 N to 305.9735 N through a change in the angle of attack from 2° to 4°.

Figure 12 provides an understanding of the variation in the drag force with respect to the angle of attack. The drag force had a significant reduction ranging from 2.3965 N to 1.8635 for the complete glider. The implementation of VGs had a drag reduction of about 0.3204 N, which was the sole purpose of VGs. Although it does not seem much, it does contribute to the overall drag reduction.

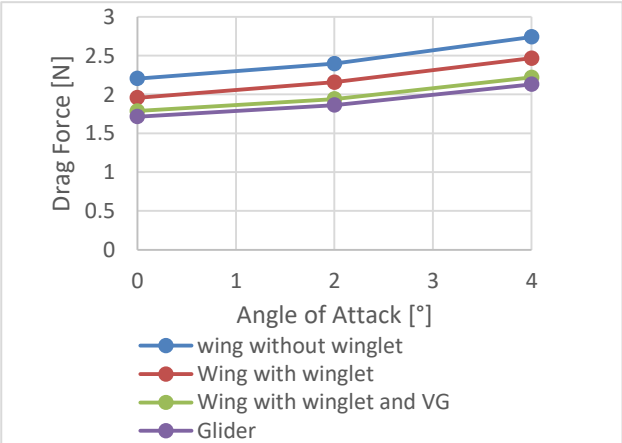

Figure 12. Drag force *vs.* AOA.

The drag force illustrates how the drag force increases with respect to the angle of attack. This is due to the dependency of the drag coefficient on the velocity magnitude, implying as the velocity of the freestream increases the drag coefficient rises accordingly [19].

6. Discussion

The main lift comes when the wing is angled so the air striking the underside of the wing gets forced downwards, which is why the lift is increasing as the angle of attack increases but the drag increases comparatively and so the motor must provide more thrust to cope up with that [20-22].

The lift and drag forces increase when the winglet is implemented on the wing. Implementing a winglet reduces the flow increasing efficiency. The drag reduces since the winglet makes the passage of air from bottom to top much difficult, which reduces the wingtip vortex, thus reducing the induced drag.

The lift increases once VG has been implemented. The reasoning behind that is that the vortex generators tend to create their own vortices; these vortices of air proceed to energize the layer of air above the wing surface, and that causes the air to remain attached to the layer much longer as AOA for the glider increases.

The lift and drag slightly increased for the final aircraft, both the coefficients, and the forces. The reasons behind the increases is the empennage. The empennage basically contributes to a very small percentage of the potential lift. The forces as well as the coefficients of lift measured from the above simulation must be doubled for the actual glider as there are two wings and the simulation are performed for one only. The simulation was performed for one in order to reduce the computation time.

7. Nomenclature

P: Pressure, Pa

ρ: Density, $\frac{kg}{m^3}$

V: Velocity, $\frac{m}{s}$

$\boldsymbol{g}$: Gravitational acceleration, $\frac{m}{s^2}$

$\boldsymbol{z}$: Vertical distance, m

L: Lift force, N

$\mathbf{C_L}$: Coefficient of lift

S: Surface area, m^2

D: Drag force, N

$\mathbf{C_D}$: Coefficient of drag

$\dot{\boldsymbol{W}}_{\boldsymbol{t}}$: Total power. W

$\mathbf{V_t}$: Total voltage, V

7. Conclusion

The solar glider was successfully designed in order to achieve a perpetual endurance flight and a clean renewable energy source. The wings were designed to fit 16 solar cells across the wingspan for a maximum energy input. The theoretical power output of the solar cells ought to be 57.6 Watts, which is stored in a 2S 7.4V 2200 mAh Li-Po battery. The ANSYS Fluent simulation provided a good basis of results on the lift and drag once VGs were implemented on the wingspan. The applications of VGs increased the lift force of the glider from 159.8 N to 191.7 N at 0° AOA; however, the concept of vortex generators requires further research works with various VG shapes and sizes. Future recommendations include:

- Testing various propeller types for assortment of an efficient setting with the intention of saving energy and providing a lengthier flight duration.
- Increasing the wing area for mounting additional solar panels intended for an extended flight duration.

8. References

[1] Eid, Saif Eldin, and Sharul Sham Dol. "Design and Development of Lightweight-High Endurance Unmanned Aerial Vehicle for Offshore Search and Rescue Operation." In 2019 Advances in Science and Engineering Technology International Conferences (ASET), pp. 1-5. IEEE, 2019.

[2] Hassanalian, M., & Abdelkefi, A. (2017). Classifications, applications, and design challenges of drones: A review. Progress in Aerospace Sciences, 91, 99-131.

[3] Muhammad Ahsan Iqbal, Abdul Qader Abdullah, Sharul Sham Dol. "Design of self-powered surveillance RC aircraft". International Journal of Engineering Research in Mechanical and Civil Engineering, 5(2), pp. 1-6, 2020.

[3] Sturm, Hannes, Gerrit Dumstorff, Peter Busche, Dieter Westermann, and Walter Lang. (2012) "Boundary Layer Separation and Reattachment Detection on Airfoils by Thermal Flow Sensors." 12. Accessed May 5, 2020.

[4] Hobbs, A., and Herwitz, S. R. (2006). "Human challenges in the maintenance of unmanned aircraft systems ". FAA and NASA Report.

[5] Houghton, E. L., P. W. Carpenter, Steven H. Collicitt, and Daniel T. Valentine (2017). Aerodynamics for Engineering Students. 7th. Elsevier.

[6] Dol, S. S., & Bin, C. H. (2019, April). Fluid-Structural Interaction Simulation of Vortices behind a Flexible Vortex Generator. In 2019 8th International Conference on Modeling Simulation and Applied Optimization (ICMSAO) (pp. 1-5). IEEE.

[7] Abid Abdul Azeez, Mohamed Gadala, Nasr Al Khudhiri, Sharul Sham Dol. "Aerodynamics Optimization of RC Plane Winglet." 2019 8th International Conference on Modeling Simulation and Applied Optimization (ICMSAO), pp. 1-5. IEEE, 2019.

[8] NASA. (2018) Shape Effects on Lift. Edited by Nancy Hall. February 5. Accessed April 20, 2020. https://www.grc.nasa.gov/www/k-12/airplane/shape.html.

[9] Siew Ping Yeong and Sharul Sham Dol. "Aerodynamic Optimization of Micro Aerial Vehicle". Journal of Applied Fluid Mechanics, Vol. 9, No. 5, pp. 2111-2121, 2016.

[10] John D. Anderson, Jr. (2010) Fundamentals of Aerodynamics. 5th. McGraw Hill.

[11] Cutler, Colin, and Mark R. Korin. (2016) "Aerodynamics of Flight." Chap. 5 in Pilot's Handbook of Aeronautical Knowledge, by John S. Duncan, 1 - 51. Philadelphia: United States Department of Transportation, Federal Aviation Administration, Airman Testing Standards Branch. Accessed April 21, 2020.

[12] Maxemow, Shane. (2009) "Thats a Drag: The Effects of Drag Forces." Undergraduate Journal of Mathematical Modeling 2 (1). Accessed April 21, 2020.

[13] Sharul Sham Dol, Mohd Arief Mohd Nor and Muhamad Khairun Kamaruzaman. "Flow visualization of the vortex shedding of a stationary circular cylinder by an improved smoke-wire technique". WSEAS Transactions on Fluid Mechanics, Issue 6, Volume 1, pp.745-752, 2006.

[14] Dol, Sharul Sham. (2019) "Aerodynamic optimization of unmanned aerial vehicle for offshore search and rescue (SAR) operation." IOP Publishing. doi:10.1088/1757-99X/715/1/012015.

[15] Castro, Francisco. (2019) What's the difference between n-type and p-type solar cells? June 4. Accessed June 20, 2020.

[16] Becker, Brett. 2019. Propeller Pitch Explained. September 27. Accessed July 7, 2020. https://www.boatingmag.com/how-to/understanding-propeller-pitch/.

[17] Anderson, J. D. (2009) "Governing Equations of Fluid Dynamics." Computational Fluid Dynamics 3. Accessed May 8, 2020.

[18] Almedeij, Jaber. 2008. "Drag coefficient of flow around a sphere." September 10: 218 - 233. Accessed June 28, 2020.

[19] Hiremath, S., & Malipatil, A. S. (2014). "CFD Simulation of Aircraft Body with Different Angle of Attack and Velocity". International Journal of

Innovative Research in Science, Engineering and Technology, 3(10).

[20] A. F. El Ghazali and S. S. Dol. "Aerodynamic Optimization of Unmanned Aerial Vehicle through Propeller Improvements." Journal of Applied Fluid Mechanics, Vol. 13, No. 3, pp. 793-803, 2020.

[21] Dol, S. S., Chan, H. B., Wee, S. K., & Perumal, K. (2020, January). The effects of flexible vortex generator on the wake structures for improving turbulence. In IOP Conference Series: Materials Science and Engineering (Vol. 715, No. 1, p. 012070). IOP Publishing.

[22] Yong, T. H., Chan, H. B., Dol, S. S., Wee, S. K., & Kumar, P. (2017, June). The flow dynamics behind a flexible finite cylinder as a flexible agitator. In IOP Conference Series: Materials Science and Engineering (Vol. 206, No. 1, p. 012033).